Effect of Heat Treatment on Creep Properties of *in situ* Synthesized (TiB+La$_2$O$_3$)/Ti Composite

Jiuxiao Li[1], Yuanfei Han[2]*, Dongye Yang[1]* and Jianwei Mao[2]

[1] School of Materials Engineering, Shanghai University of Engineering Science, Shanghai, China, [2] State Key Laboratory of Metal Matrix Composites, Shanghai Jiao Tong University, Shanghai, China

(TiB+La$_2$O$_3$)/IMI834 titanium matrix composites (TMCs) were developed by *in situ* synthesized in a consumable vacuum arc-remelting furnace. A new TRIPLEX treatment and β heat treatment were developed in this study. The effect of heat treatment on microstructure, tensile properties and creep rupture behavior of *in situ* synthesized (TiB+La$_2$O$_3$)/IMI834 titanium matrix composites (TMCs) and corresponding matrix alloy were investigated. The results show that widmanstätten and lamellar α structure formed after the new TRIPLEX heat treatment procedures. Compared with traditional β heat treatment, the creep strain rate increases slightly, but the elongation increases significantly (increase 126% at 293 K, 59.13% at 873 K). The fracture mechanism is attributed to the broken of TiB whiskers after bearing high stress. The creep fracture mechanism is due to the load transfer of TiB whiskers and interfacial debonding. The Creep strain rates of TMCs are lower than that of matrix alloy, which is attribute to that loading of TiB and the pinning effect of finer La$_2$O$_3$ particles on dislocation movement.

Keywords: titanium matrix composites, reinforcement, microstructure, creep, strengthening mechanism

INTRODUCTION

Continuous/discontinuous reinforcements could be used to greatly improve the mechanical properties of Ti and Ti-alloys by different processing routes (Imayev et al., 2014; Liu et al., 2018). In these several decades, *in situ* synthesized Ti matrix composites (TMCs) are proved to have superior mechanical properties compared with those of matrix Ti alloy (Wang et al., 2015; He et al., 2017; Ma et al., 2018; Vasanthakumara et al., 2019). The near-α IMI834 Ti alloy has good combination of creep and fatigue resistance at elevated temperatures, service temperatures up to 873 K, which is developed primarily for rotating components in the compressor part of advanced jet engines (Ghavam et al., 2015; Li et al., 2018; Zhang and Chen, 2018). Therefore, IMI834 is best candidate as matrix alloy, which is reinforced with ceramic particles are investigated in detail.

As is well-known, the service life and safety reliability are important for high temperature Ti alloy (Su et al., 2018). Creep rupture behavior is one of the most important considered factors for evaluating the quality of high-temperature Ti alloys (Balasundar et al., 2014; Jiao et al., 2017). Ti alloys will undergo elastic deformation during long-term creep at high temperatures, when the elastic deformation accumulates to the limitation, plastic deformation would occur and eventually fails, as the plastic deformation increases (Nie et al., 2016). From the literature review, IMI834 and TMCs are designed as high-temperature structural material, it is necessary to focus on the creep resistance for long time service. Especially on the investigation of microstructural evolution during the creep deformation process. It is important for understanding the creep properties

determined by the forming and heat treatment (Hosseini et al., 2017; Ozerov et al., 2019). The bimodal microstructure consists of equiaxed α grains and α+β colonies, creep strain rates reduce with equiaxed α decreasing in bimodal microstructure during primary and secondary creep. The widmanstätten structure treated by β heat treatment, consists of α+β colonies in β grain. The widmanstätten structures have better creep resistance and worse ductility, compared with those of bimodal microstructures (Zhang et al., 2010; Liu et al., 2019; Wang et al., 2019). Therefore, the comprehensive mechanical properties could be improved by the optimum heat treatment processing.

In this study a new TRIPLEX heat treatment method is developed to improve the comprehensive mechanical properties. The microstructural characteristics of IMI834 and TMCs after β and TRIPLEX heat treatment were investigated, respectively. It will deepen the quantitative understanding of the relationship between microstructural features and creep rupture properties.

EXPERIMENTAL PROCEDURE

The near α high temperature Ti alloy IMI834 (Ti-5.8Al-4Sn-3.5Zr-0.7Nb-0.5Mo-0.35Si-0.06C wt%) is adopted as matrix alloy. TiB short fibers and La_2O_3 particles are synthesized via internal reaction during the vacuum arc re-melting: $12Ti + 2LaB_6 + 3[O] = 12TiB+La_2O_3$. The volume fraction of TiB and La_2O_3 is designed as 1.8 and 0.6 V%, respectively. *In situ* synthesized $(TiB+La_2O_3)/Ti$ composites (TMCs) and matrix alloy IMI834 were prepared in a consumable vacuum arc melting furnace. The ingots were hot forged into Φ15 mm in diameter. The beta transformation temperature of matrix alloy and TMCs are ~1303, 1313 K.

Heat treatment procedure for matrix alloy and TMCs of this paper are β heat treatment (HT1), TRIPLEX heat treatment (HT2).

- β heat treatment (HT1): air cooling (AC) in β phase region (1328 K, 0.5 h/AC), then aging (923 K, 2 h/AC).
- TRIPLEX heat treatment (HT2): β solution [1328 K, 0.5 h/oil quenching (OQ)], α+β solution (1248 K, 1 h/AC), and then aging (923 K, 2 h/AC).

Room temperature tensile tests were performed on Zwick T1-Fr020TN testing machine. High temperature tensile tests were performed on CSS-3905 testing machine. The gauge section size of the tensile specimens is 15 × 4 × 1.5 mm. The strain rate of tensile tests is $10^{-3}s^{-1}$ at room temperature, 873, 923, and 973 K, respectively. The creep rupture properties were tested on CSS-3905 testing machine in air at 873, 923, and 973 K, respectively. The temperature was controlled by three thermocouples placed at the top, center, and bottom position of the specimen, and the fluctuations were controlled in ± 0.2 K. Creep specimens were cut in the hot forging direction. The creep specimens gauge size is Φ 5 × 25 mm. The tensile and creep tests specimens were fabricated in the hot forged rods by using wire electrical discharge machining. Each specimen was ground using SiC papers up to 2,000 grits and then polished using a polishing cloth.

Microstructure was observed by optical microscope (OM). The reinforcements (TiB whiskers and La_2O_3) were observed by JEM-2000 EX transmission electron microscopy (TEM), and JSM-6700F scanning electron microscope (SEM) was used to observe electron backscattered diffraction (EBSD) and fracture surfaces of specimens after tensile and creep tests. The SEM specimen were ground using SiC papers up to 2,000 grits and then polished using a polishing cloth according to standard metallographic procedures. Specimens for EBSD and TEM were prepared by electropolishing.

# RESULTS AND DISCUSSION

Microstructure

Figure 1 shows the microstructures of matrix alloy and TMCs after heat treatment. The microstructure of matrix alloy and TMCs is widmanstätten (**Figures 1A,C**) after HT1, and the microstructure shows lamellar structure (**Figures 1B,D**) after HT2 for matrix alloy, TMCs. Lamellar α morphology and size are affected by the heat treatment processing parameters, such as heating temperature, holding time, cooling rate (Guo and Baker, 1992). As the cooling rate increasing, the lamellar α thickness generally decreases and lamellar structure changed into basketweave and martensite structure. Rapid cooling would resulted in the formation of martensite structure during the Oil or water quenching process. Low cooling rates result in formation of coarse α lamellar (Wang et al., 2006). The HT2: oil quenched in β phase region, the fine and acicular martensite forms. if air cooled in α+β phase region, the martensite would decompose into fine acicular and coarse α phase, thus, α+β colony size of matrix alloy and TMCs is much longer, thinner than those HT1 procedure. The TiB whiskers are observed in **Figures 1C,D**, which aligned along the forging direction. TiB whiskers will rotate and gradually parallel to the direction of deformation during hot deformation (Ma et al., 2016, 2017a).

Figure 2 shows EBSD microscopy of TMCs after heat treatment. The blocks are α+β colonies. The lamellar α with nearly the same orientation is labeled by the same color. In **Figure 2A**, the larger α+β colonies are marked as large, differently colored areas in widmanstätten treated by HT1. **Figure 2B** shows EBSD microscopy of TMCs after HT2. The aspect ratio of α+β colonies treated by HT2 is larger than that of HT1 procedure. The percentage of high angle boundaries in TMCs treated by HT2 is larger than that of HT1, few larger α+β colonies are identified in **Figure 2B**.

Figure 3 shows misorientations of TMCs after different heat treatment procedure. The colored lines are the misorientation angles (θ) between neighboring grains. The green lines represent low angle boundaries in $2 < θ < 17°$, other colors are high angle grain boundaries in $θ > 17°$. The grain boundaries between α/α lamella are low angle boundaries in α+β colony. The boundaries of α/α grains, α/α+β colony and α+β colony are high angle boundaries (Li et al., 2016). Most low angle boundaries are in the high angle boundaries, which is observed in **Figures 3A,B**. **Figures 3C,D** shows the number of misorientations of TMCs after heat treatment. The percent of low angle boundaries in
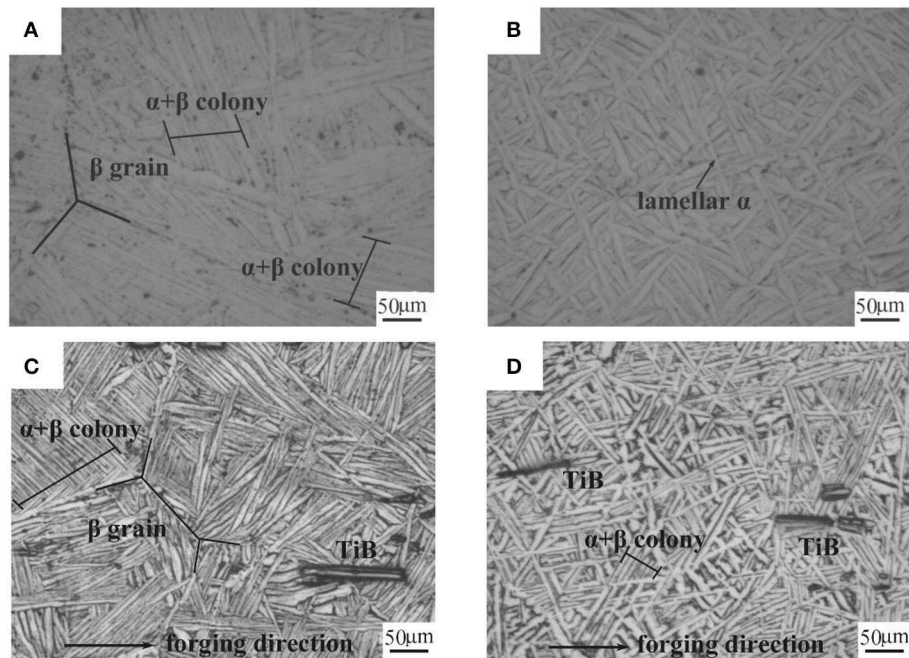
FIGURE 1 | The microstructure of specimens after heat treatment. (A) Matrix alloy, HT1. (B) Matrix alloy, HT2. (C) TMCs, HT1. (D) TMCs, HT2.
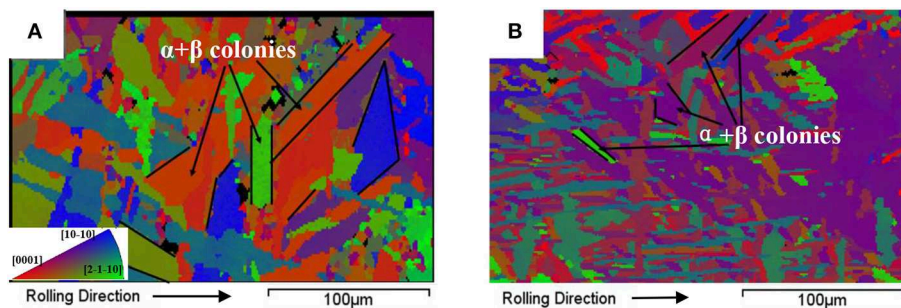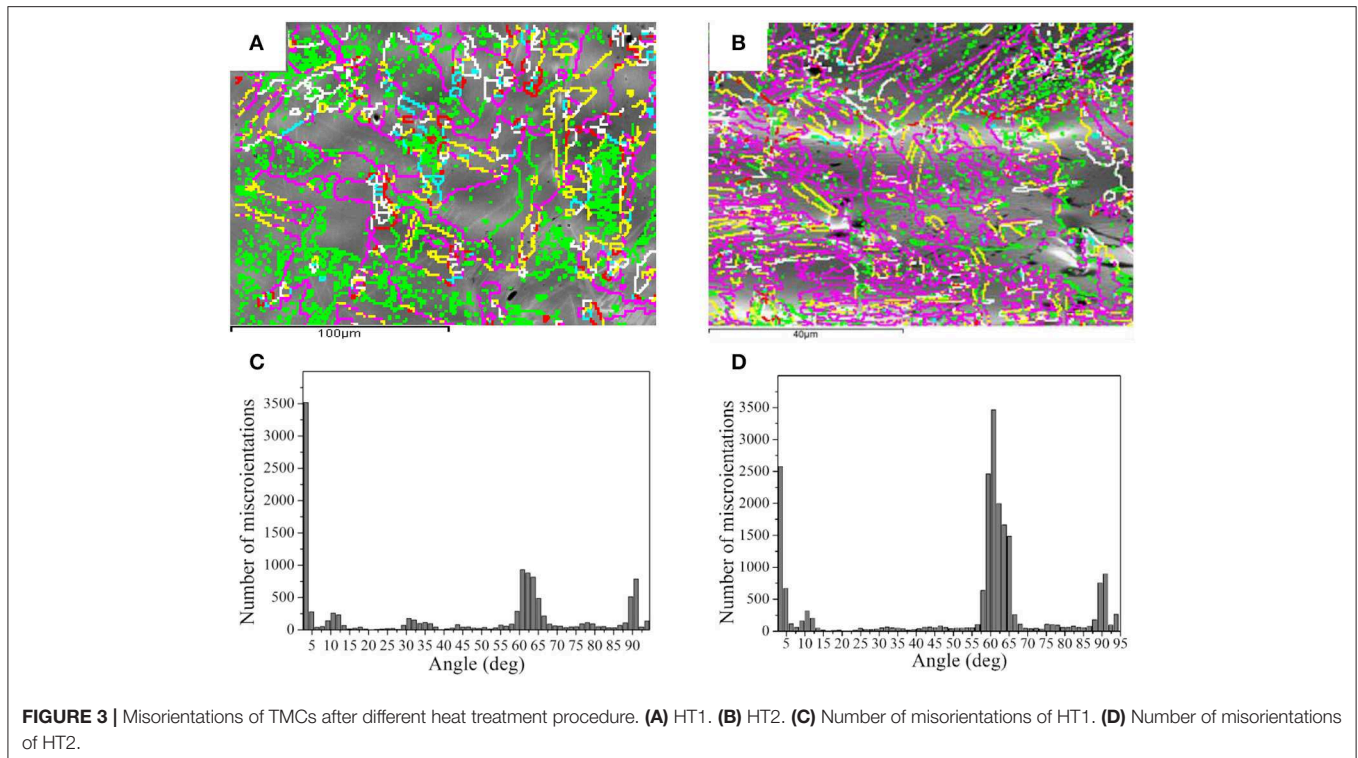

FIGURE 2 | EBSD microscopy of TMCs after heat treatment. (A) HT1. (B) HT2.

TMCs treated by HT2 significantly is lower than that of HT1, which is observed in **Figures 3A–D**.

Tensile Properties

Figure 4 shows the yield strength and elongation of matrix alloy and TMCs after heat treatment at room temperature. The yield strength of matrix alloy after HT2 increases 0.5% (1073 ± 20 MPa) than that of HT1 (1068 ± 25 MPa), the elongation improves 100% (from 5 ± 1.5% HT1 to 10 ± 3% HT2). The change of room temperature tensile property of TMCs appears the same trend with that of matrix alloy. The yield strength of TMCs after HT2 (1,125 ± 28 MPa) increases 0.9%, the elongation (16 ± 3%) improves 128%, compared with those of HT1 (1,115 ± 22 MPa, 7 ± 2%). The yield strength and elongation of TMCs are better than the matrix alloy.

The high temperature ultimate strength and elongation of heat-treated matrix alloy and TMCs are shown in **Figure 5**. The all ultimate strength decreases, while the elongation increases, with the temperature increasing. The ultimate strength and elongation of matrix alloy treated by HT1 is 711 ± 25 MPa, 20 ± 4% 873 K, 595 ± 18 MPa, 23 ± 4.5% 923 K, and 423 ± 15 MPa, 44 ± 5% 973 K, respectively. The ultimate strength of matrix alloy treated by HT2 changes slightly, while elongation improves significantly, increase about 25, 35, and 41% from 873 to 973 K, respectively, compared with those of HT1. The ultimate strength and elongation of TMCs treated by HT1 is 799 ± 20 MPa, 22 ± 3%, 735 ± 19 MPa, 28 ± 5% or 652 ± 15 MPa, 56 ± 4% at 873, 923, and 973 K, respectively. The ultimate strength of TMCs treated by HT2 changes slightly, while elongation improves significantly, increase about 59, 28, and 31% from 873 to 973 K, respectively, compared with those of HT1. The ultimate

FIGURE 3 | Misorientations of TMCs after different heat treatment procedure. **(A)** HT1. **(B)** HT2. **(C)** Number of misorientations of HT1. **(D)** Number of misorientations of HT2.

strength of TMCs is higher than that of matrix alloy. Significantly, which increased by about 12, 26, and 50% treated by HT1 at 873, 923, and 973 K. The ultimate strength and elongation of TMCs improve significantly at high temperature, compared with those of matrix alloy. The tensile properties of HT2 are superior to that of HT1 at high temperatures.

Because the microstructures treated by HT1 and HT2 are α+β colonies, and the reinforcement morphology have no changes before and after HT1 and HT2, the same results are observed in the near fracture surfaces, as shown in the SEM image of HT1 and HT2 after tensile test. Only two images are used to discuss the results. **Figure 6A** shows a SEM image of matrix alloy near fracture surfaces after tensile test at 923 K. Most lamellar α grain boundaries are continuous, and both transgranular and intergranular cracks are observed in **Figure 6A**. A SEM image of TMC near fracture surfaces after tensile test at 923 K is shown in **Figure 6B**. The lamellar α grain boundaries are continuous, and some broken TiB whiskers are observed near the tensile fracture in **Figure 6B**. The stress is easily transferred from matrix to TiB whiskers in the tensile test process, TiB whiskers would load intensive stress, and broken as the load increases, which is the typical fracture mechanism of TMCs in reinforcement TiB whisker (Gorsse and Miracle, 2003; Boehlert et al., 2006; Ma et al., 2017b).

Creep Properties

As is well-known, creep strain rate is the strain rate in the steady-state creep stage, when the temperature and stress are low. The minimum strain rate is creep strain rate when temperature and stress are high. **Figure 7** shows the creep strain rate of matrix

alloy and TMCs after heat treatment. As the temperature or stress increases, the steady-state creep strain rate also increases.

The creep strain rates of matrix alloy and TMCs after HT2 increase slightly compared with those of HT1, but the creep strain rate is in the same range magnitude except matrix alloy at 973 K/80 MPa, TMCs 973 K/200 MPa. Compared with matrix alloy, the creep strain rate of TMCs decreases, especially decreases one magnitude at 973 K 150 MPa (TMCs 10^{-7}, matrix alloy 10^{-6}), 873 K 200 MPa (TMCs 10^{-9}, matrix alloy 10^{-8}), 923 K 200 MPa (TMCs 10^{-8}, matrix alloy 10^{-7}). The creep strain rates of TMC are significantly lower than those of matrix alloy due to reinforcements added in TMCs.
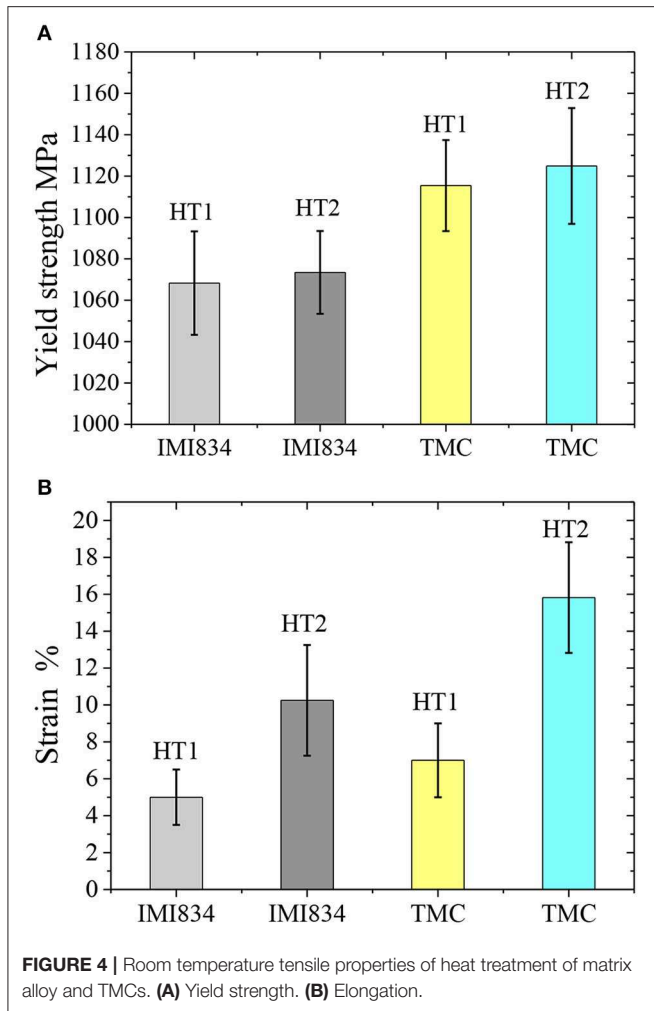
The relationship between creep rate and stress and temperature can be expressed by the following Equations (1–3) (Li et al., 2008; Wang et al., 2009, 2019):

$$\dot{\varepsilon} = A\sigma^n \exp\left(-\frac{Q}{RT}\right) \tag{1}$$

$$n = \frac{d\ln\dot{\varepsilon}}{d\ln\sigma} \tag{2}$$

$$Q = -R\frac{d\ln\dot{\varepsilon}}{d\frac{1000}{T}} \tag{3}$$

Where $\dot{\varepsilon}$ is the creep strain rate of specimen, A is a material constant, σ is the applied stress added during creep test, n is the

FIGURE 4 | Room temperature tensile properties of heat treatment of matrix alloy and TMCs. **(A)** Yield strength. **(B)** Elongation.

FIGURE 5 | High temperature tensile properties of matrix alloy and TMCs after heat treatment. **(A)** Ultimate strength. **(B)** Strain.

stress exponent, Q is the activation energy, R is the gas constant and T is the Kelvin temperature. According to Equation (2), apparent stress exponents can be determined by the Arrhenius plot of logarithmic $\dot{\varepsilon}$ vs. stress. According to Equation (2), ln $\dot{\varepsilon}$ and ln σ are linear at the same temperature, and the slope of straight line is the apparent stress exponents.
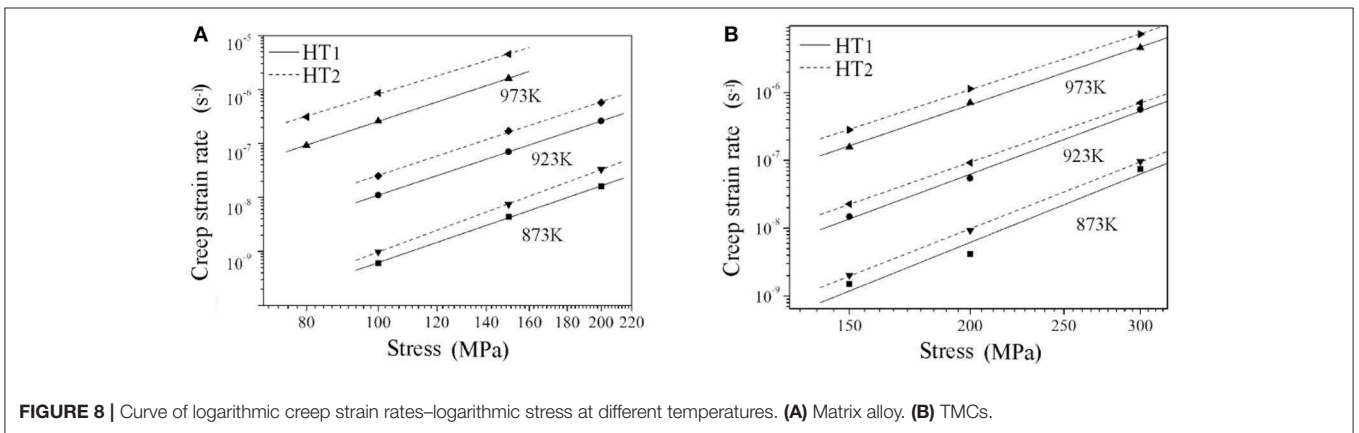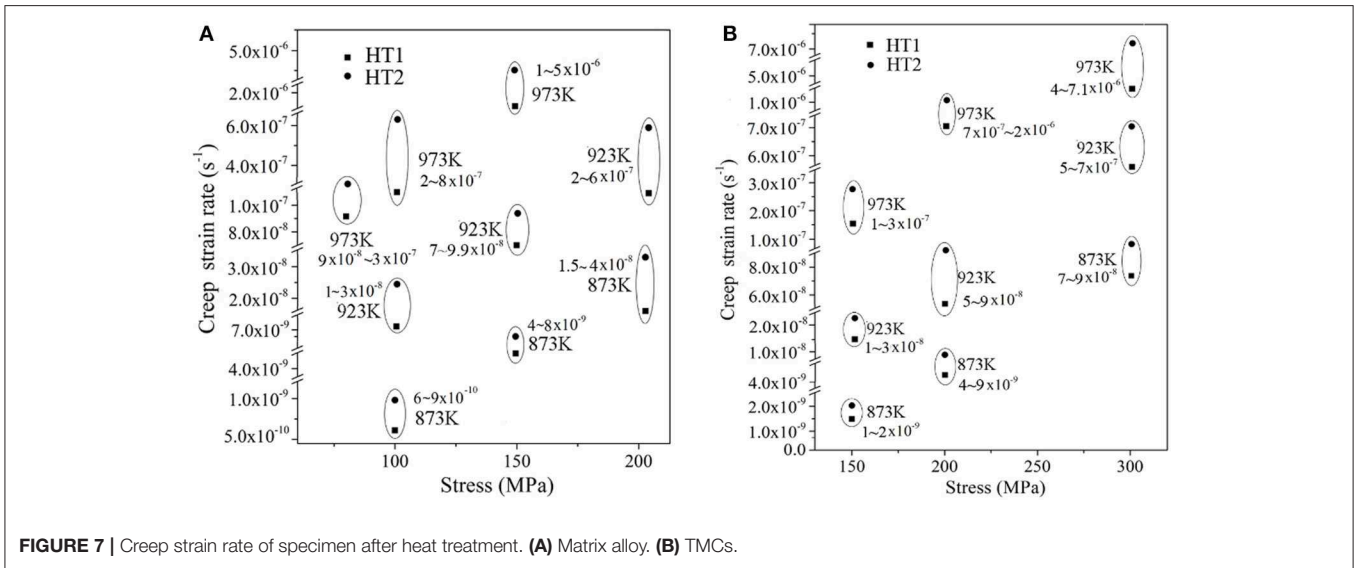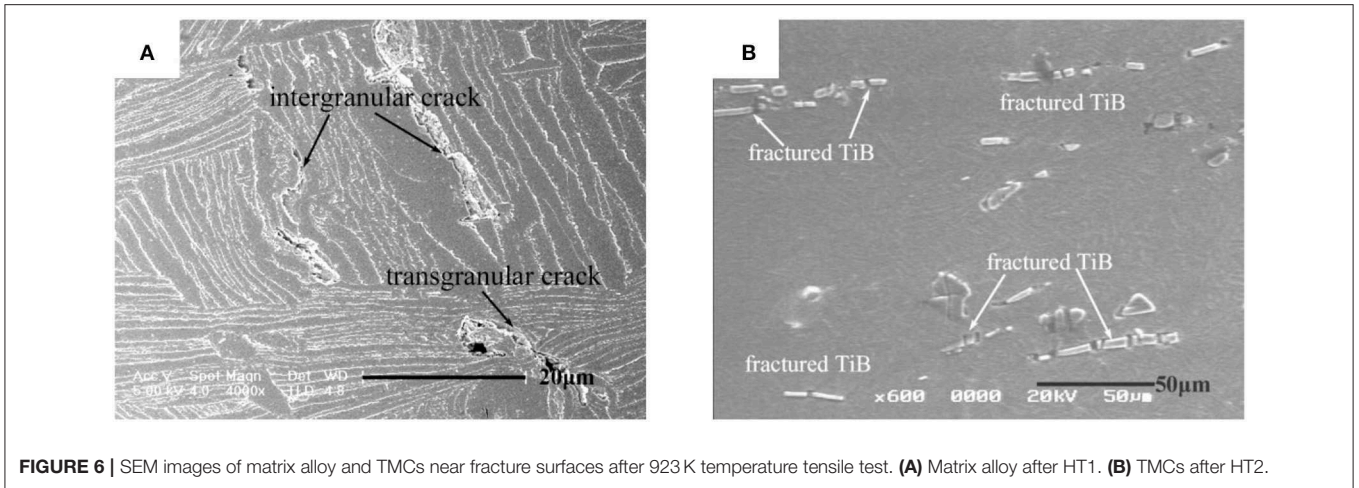
Figure 8 show the curve of logarithmic creep strain rates– logarithmic stress of matrix alloy and TMC. According to the slope of straight line in **Figure 8A**, apparent stress exponents of matrix alloy treated by HT1 and HT2 are 4.6, 4.5 at 923 K, respectively. Effects of heat treatment and temperature on the apparent stress exponents are not significant in matrix alloy. According to the slope of straight line in **Figure 8B**, apparent stress exponents of TMCs treated by HT1 and HT2 are 5.3, 5.0 at 923 K, respectively. Apparent stress exponents decrease with temperature increasing. The apparent stress exponents of matrix alloy are lower than those of TMCs. Wang et al. (2009) have reported that the creep behavior can be divided into two categories: one creep behavior controlled by viscous dislocation sliding is different; other creep behavior controlled by dislocation climb. Koike et al. (1995) report that dislocation
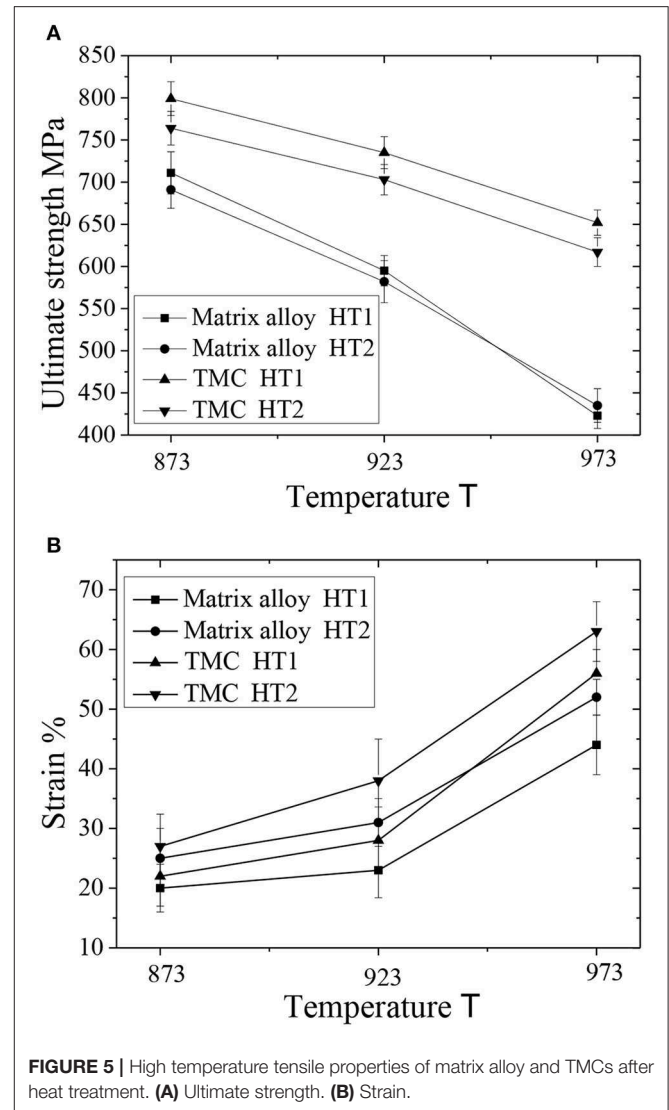
sliding is dominant when the stress exponent is 3.5, when the stress exponent is 4.6, dislocation climb is governing.

The activation energy can be deduced by the curve of logarithmic $\dot{\varepsilon}$–reciprocal Kelvin temperature 1,000/T at constant stress, according to Equation (3). **Figure 9** shows the activate energy of the matrix alloy and TMCs at constant stresses. The activation energies of matrix alloy treated by HT1 and HT2 are 357 kJ/mol, 350 kJ/mol at 150 MPa. The activation energies of TMCs treated by HT1 and HT2 are 387 kJ/mol, 379 kJ/mol at 200 MPa. The activation energies of matrix alloy are lower than those of TMCs.

The creep resistance of Ti alloy increases with the increasing of average grain sizes. Creep strain rates are higher due to the grain boundary sliding increases in small grained Ti alloy (Sastry et al., 1980). Moreover, Ti alloys absorb oxygen in process of long-term creep in the air. The oxygen content increases with grain size decreasing in Ti alloy. The elongation and

FIGURE 6 | SEM images of matrix alloy and TMCs near fracture surfaces after 923 K temperature tensile test. (A) Matrix alloy after HT1. (B) TMCs after HT2.

FIGURE 7 | Creep strain rate of specimen after heat treatment. (A) Matrix alloy. (B) TMCs.

FIGURE 8 | Curve of logarithmic creep strain rates–logarithmic stress at different temperatures. (A) Matrix alloy. (B) TMCs.

creep resistance decrease significantly, when oxidation content increases in Ti alloy (Pitt et al., 2004). The grain and α+β colonies size of HT2 sample are smaller than those of HT1.

So, the creep resistance of HT2 is much lower. The α+β colonies and lamellar α of TMCs are finer than those of matrix alloy, but the creep properties of TMCs is higher than
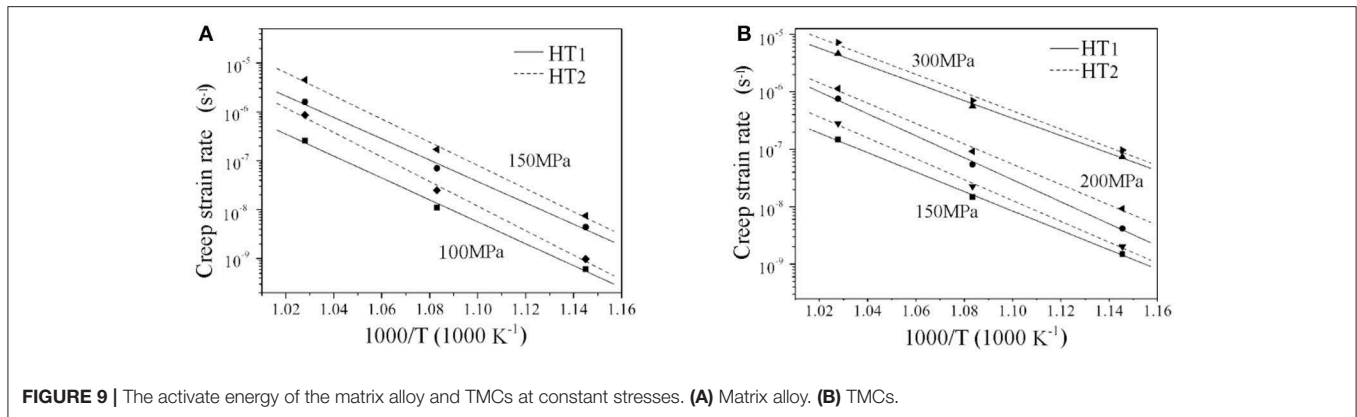
FIGURE 9 | The activate energy of the matrix alloy and TMCs at constant stresses. **(A)** Matrix alloy. **(B)** TMCs.
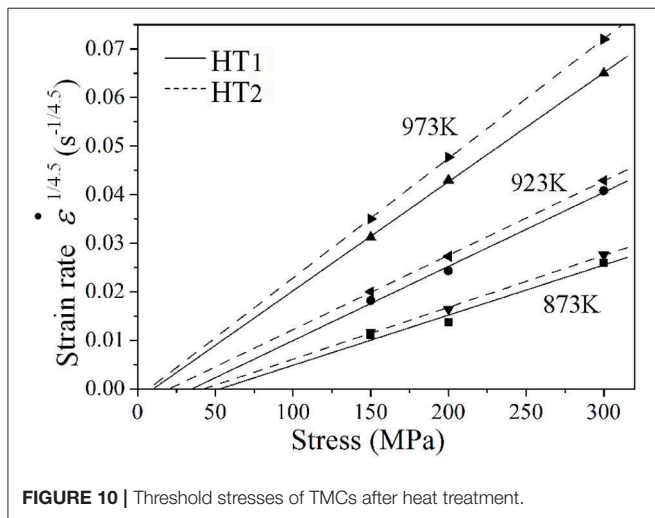

FIGURE 10 | Threshold stresses of TMCs after heat treatment.

that of matrix alloy, due to the hard reinforcements added in matrix alloy.

The apparent stress exponents of TMCs are higher than that of matrix alloy, because of threshold stress in TMCs. The abscissa intersection of the $\dot{\varepsilon}^{1/n} - \sigma$ curve is the threshold stress. Threshold stresses of TMCs after heat treatment are shown in **Figure 10**. The value of true stress exponent n is usually considered as stress exponent of matrix alloy (Wang et al., 2009; Xiao et al., 2009). The stress exponent n value of matrix alloy is all close to 4.5, which is considered that creep mechanism is the typical dislocation climbing (Hofmann et al., 1998). So, the true stress exponent value is set as 4.5, then this value $n = 4.5$ is used to calculate the threshold stress of TMCs. **Figure 10** shows good linear relationships between $\varepsilon^{1/4.5}$ and σ, which indicate that choosing true stress exponent of TMCs $n = 4.5$ is reasonable. The threshold stress decreases with the temperature increasing. The threshold stresses of TMCs treated by HT1 are bigger than those of HT2. Creep properties of TMCs are still better than that of matrix alloy, it is attributed to the TiB whiskers and La_2O_3 particles, which is considered as main reason for the generation of threshold stress.
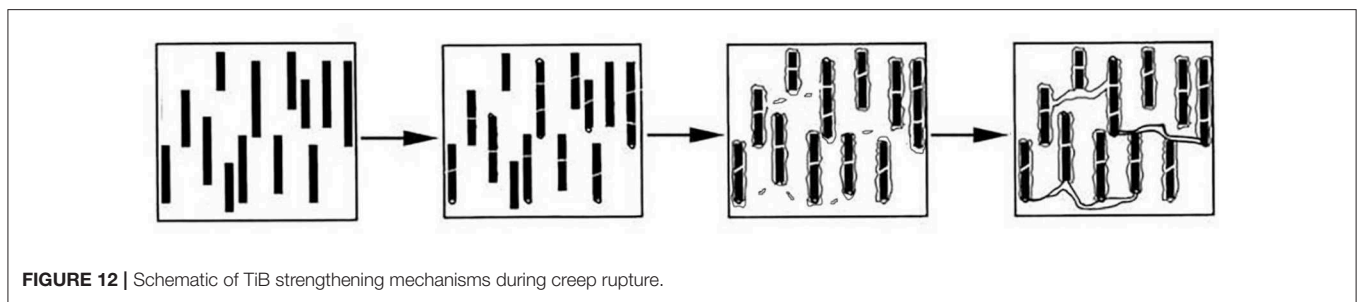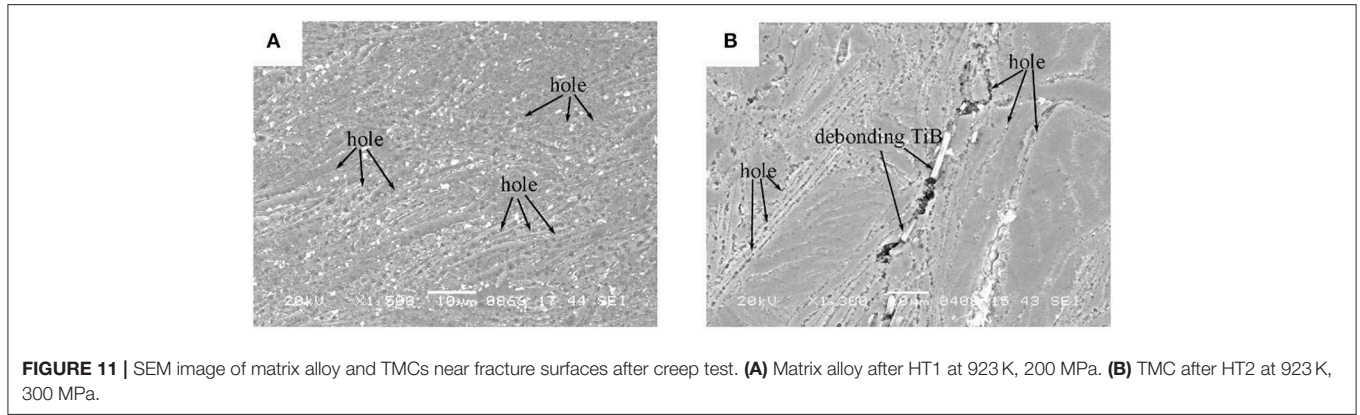
Reinforcements

The similar results are observed in the near fracture surface SEM images of HT1 and HT2 after creep test. Two images are used to discuss the change of grain boundaries and the strengthening mechanism of TiB whiskers. The microstructure of matrix alloy treated by HT1 near fracture surfaces after 923 K/200 MPa creep fracture test is shown in **Figure 11A**. The grain boundaries of lamellar α become discontinuous, and a lot of cavies are formed on grain boundaries. The creep fracture is attributed to the disintegration of lamella α boundaries. The great deformations and bending lamellar α near fracture surfaces after creep test can be observed in **Figure 11A**. The grain boundary strength decreases, as the exposure time at high temperature increases, so the fracture mechanism of creep becomes intergranular crack (Es-Souni, 2000; Wang et al., 2006). **Figure 11B** shows SEM image of near fracture surfaces for TMC treated by HT2 after 923 K, 300 MPa creep fracture test. The lamellar α grain boundaries become discontinuous. Some crack and interfacial debonding of TiB whiskers and intergranular cracks are observed in **Figure 11B**. The TiB interfacial debonding indicated that the interface strength decreased after exposure for a long time at high temperature.

TiB reinforcements take load from the matrix, and then break. A coefficient β can be indicated the effect of load transfer by following equations (Wang et al., 2009):

$$(1 - \beta)^n = \frac{\dot{\varepsilon}_c}{\dot{\varepsilon}_m} \qquad (4)$$

Where n is the true stress exponent. ε_c and ε_m are the creep strain rate of the matrix and composite, respectively. The coefficient β indicates effect of load transfer from matrix to reinforcement. The β value is 0–1(the β value of matrix is 0). The stress of TMCs and load transfer coefficient can be expressed as the following equations (Wang et al., 2009; Xiao et al., 2009):

$$\overline{\sigma}_r = E_r \varepsilon_0 \left[1 - \frac{\tan h\,(ps)}{ps} \right] \qquad (5)$$

FIGURE 11 | SEM image of matrix alloy and TMCs near fracture surfaces after creep test. **(A)** Matrix alloy after HT1 at 923 K, 200 MPa. **(B)** TMC after HT2 at 923 K, 300 MPa.

FIGURE 12 | Schematic of TiB strengthening mechanisms during creep rupture.

$$\sigma_0 = \overline{\sigma}_r v_r + \overline{\sigma}_m v_m = \varepsilon_0 \left\{ v_r E_r \left[1 - \frac{\tan h\,(ps)}{ps} \right] + (1 - v_r)\, E_m \right\} \quad (6)$$

$$\beta = \frac{\overline{\sigma}_r v_r}{\sigma_0} = \frac{v_r E_r \left[1 - \tan h\,(ps)\,/ps \right]}{v_r E_r \left[1 - \tan h\,(ps)\,/ps \right] + (1 - v_r)\, E_m} \quad (7)$$

Where E_r is elastic modulus of the reinforcement, E_m is elastic modulus of the matrix alloy, $\overline{\sigma}$ is the average transferred stress, ε_0 is the strain, v_r is the reinforcement volume percent, p and s are geometric shape parameters of the reinforcements. E_m decreases with temperature rising (Wang et al., 2009). From Equations (5–7), it can deduce that with temperature rising, β increases, threshold stress decreases, load transfer increases, and the strengthening mechanism changes from threshold stress to load transfer.

Figure 12 show the schematic of TiB strengthening mechanisms during creep rupture. As the creep test progresses, the TiB whiskers take load from the matrix and crack, then debonding from matrix and intergranular cracks appears (Rabadia et al., 2018). These cavities around debonding TiB whiskers and intergranular cracks cause stress concentration, which prompts TMCs fracture during accelerating creep process.

Figure 13 shows bright field the TEM microscopy and diffraction pattern of La_2O_3 particles after creep at 923 K, 300 MPa. The synthesized dispersed small La_2O_3 particles make the dislocation pile-ups around their boundaries (**Figure 13**). The precipitation hinders dislocation motion. The strengthen increases by dislocation

FIGURE 13 | Bright field TEM microscopy and diffraction pattern of La_2O_3 particles after creep at 923 K, 300 MPa.
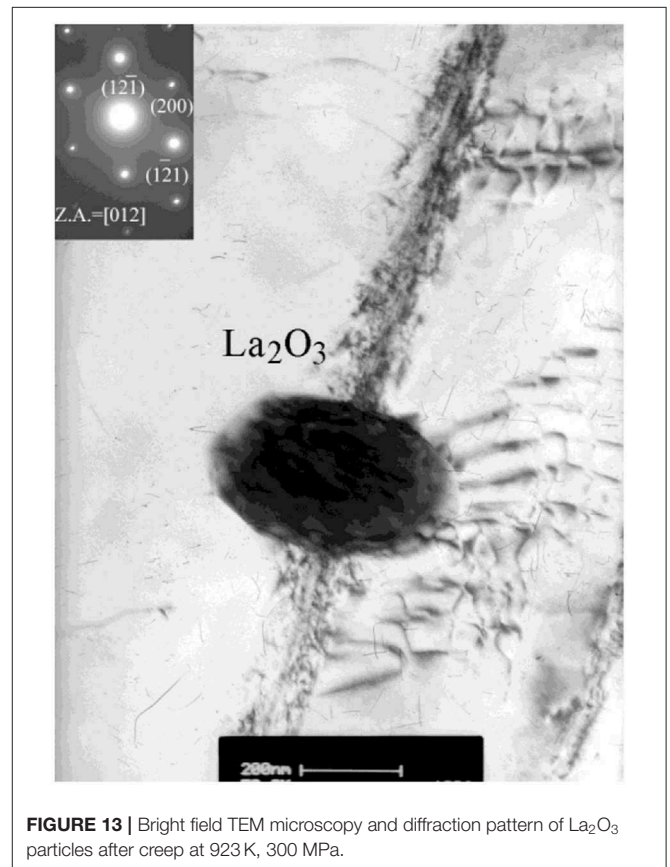
pinning (Rabadia et al., 2019). The dislocation density is effective enhanced by La_2O_3 particles, and then creep resistance improved, which is explained by Orowan stress.

The Orowan stress can be calculated by using equations (Kawabata et al., 2004):

$$\tau_o = Gb/\lambda \qquad (8)$$

Where G is the shear modulus, b is the Burgers Vector, λ is the average distance between reinforcement particles. Other La can reduce oxygen content in Ti alloys, which is helpful to improve the mechanical properties of Ti alloys.

Creep properties of TMCs are still better than that of matrix alloy. Strengthening mechanisms of reinforcements is the TiB whiskers take load from the matrix and the dislocation movement is pinned by fine La_2O_3 particles during creep procedure.

CONCLUSIONS

The effect of β heat treatment (HT1) and a new TRIPLEX heat treatment (HT2) on creep properties of IMI834 and TMCs has been conducted. This study shows the following conclusions.

(1) The widmanstätten structure is formed by HT1 for IMI 834 and TMCs, lamellar α structure is formed by HT2. The proportion of low angle boundaries of TMCs treated by HT2 (22%) is lower than that of HT1 (26%).

(2) The creep resistance of HT2 drops slightly, but elongation enhances significantly. The lamellar α microstructure of IMI834 and TMCs overcomes the shortcomings of HT1, and an optimum combination of creep and tensile properties is obtained.

(3) Creep resistance of TMCs is higher than that of matrix alloy, which is attribute to that the TiB whiskers take load from the matrix and crack, then debonding from matrix, and La_2O_3 particles pin the dislocation movement. This is strengthening mechanisms of TMCs during creep.

DATA AVAILABILITY STATEMENT

All datasets generated for this study are included in the article/supplementary material.

AUTHOR CONTRIBUTIONS

JL and YH designed experiments. JL, JM, and DY carried out experiments. JL, YH, and DY analyzed experimental results and wrote the manuscript.

FUNDING

REFERENCES

Balasundar, I., Raghu, T., and Kashyap, B. P. (2014). Correlation between microstructural features and creep strain in a near-α titanium alloy processed in the α+β regime. *Mater. Sci. Eng. A* 609, 241–249. doi: 10.1016/j.msea.2014.04.079

Boehlert, C. J., Cowen, C. J., Tamirisakandala, S., Mceldowney, D. J., and Miracled, D. B. (2006). *In situ* scanning electron microscopy observations of tensile deformation in a boron -modified Ti-6Al-4V alloy. *Scripta. Mater.* 55, 465–468. doi: 10.1016/j.scriptamat.2006.05.008

Es-Souni, M. (2000). Primary, secondary and anelastic creep of a high temperature near a-Ti alloy Ti6242Si. *Mater. Charact.* 45, 153–164. doi: 10.1016/S1044-5803(00)00069-3

Ghavam, M. H., Morakabati, M., Abbasi, S. M., and Badri, H. (2015). Flow behavior modeling of IMI834 titanium alloy during hot tensile deformation. *Trans. Nonferrous Met. Soc. China.* 25, 748–758. doi: 10.1016/S1003-6326(15)63660-3

Gorsse, S., and Miracle, D. B. (2003). Mechanical properties of Ti-6Al-4V/TiB composites with randomly oriented and aligned TiB reinforcements. *Acta Mater.* 51, 2427–2447. doi: 10.1016/S1359-6454(02)00510-4

Guo, Z. X., and Baker, T. N. (1992). On the microstructure and thermomechanical processing of titanium alloy IMI685. *Mater. Sci. Eng. A* 156, 63–76. doi: 10.1016/0921-5093(92)90416-X

He, B. B., Chang, K., Wu, W. H., and Zhang, C. L. (2017). The formation mechanism of TiC reinforcement and improved tensile strength in additive manufactured Ti matrix nanocomposite. *Vacuum* 143, 23–27. doi: 10.1016/j.vacuum.2017.05.029

Hofmann, H., Frommeyer, G., and Derder, C. (1998). Creep mechanisms in particle strengthened α-Titanium–Ti2Co alloys. *Mater. Sci. Eng. A* 245, 127–134. doi: 10.1016/S0921-5093(97)00714-4

Hosseini, R., Morakabati, M., Abbasi, S. M., and Hajari, A. (2017). Development of a trimodal microstructure with superior combined strength, ductility and creep-rupture properties in a near alpha titanium alloy. *Mater. Sci. Eng. A* 696, 155–165. doi: 10.1016/j.msea.2017.04.068

Imayev, V., Gaisin, R., Gaisina, E., Imayev, R., Fecht, H.-J., and Pyczak, F. (2014). Effect of hot forging on microstructure and tensile properties of Ti-TiB based composites produced by casting. *Mater. Sci. Eng. A* 609, 34–41. doi: 10.1016/j.msea.2014.04.091

Jiao, X. Y., Liu, G., Wang, D. J., and Wu, Y. (2017). Creep behavior and effects of heat treatment on creep resistance of Ti-22Al-24Nb-0.5Mo alloy. *Mater. Sci. Eng. A* 680, 182–189. doi: 10.1016/j.msea.2016.10.052

Kawabata, K., Sato, E., and Kuribayashi, K. (2004). Observation of weakened and strengthened creep behavior in Ti/TiB(w) composites at high temperatures. *Mater. Sci. Eng. A* 387–389, 623–627. doi: 10.1016/j.msea.2004.01.106

Koike, J., Egashira, K., Maruyama, K., and Oikawa, H. (1995). "Titanium '95 - science and technology," in *Proceedings of the Eighth World Conference on Titanium*, ed. by P. A. Blenkinsop, W. J. Evans, and E. M. Flower (Birmingham), 348.

Li, H., Zhao, Z. L., Ning, Y. Q., Guo, H. Z., and Yao, Z. K. (2018). Characterization of microstructural evolution for a near-α titanium alloy with different initial lamellar microstructures. *Metals* 8:1045. doi: 10.3390/met8121045

Li, J. X., Han, Y. F., Wang, L. Q., Chen, L. Y., and Lu, W. J. (2016). Enhanced ductility of *in situ* synthesized (TiB + La2O3)/IMI834 composite by TRIPLE heat treatment. *Mater. Trans.* 57, 1691–1697. doi: 10.2320/matertrans.M2015268

Li, Y. G., Xiao, L., Lu, W. J., Qin, J. N., and Zhang, D. (2008). Creep rupture property of *in situ* synthesized (TiB + La2O3)/Ti composite. *Mater. Sci. Eng. A* 488, 415–419. doi: 10.1016/j.msea.2007.11.028

Liu, Y. J., Li, S. J., Zhang, L. C., Hao, Y. L., and Sercombe, T. B. (2018). Early plastic deformation behaviour and energy absorption in porous β-type biomedical titanium produced by selective laser melting. *Scripta Mater.* 153, 99–103. doi: 10.1016/j.scriptamat.2018.05.010

Liu, Y. J., Zhang, Y. S., and Zhang, L. C. (2019). Transformation-induced plasticity and high strength in beta titanium alloy manufactured by selective laser melting. *Materialia* 6:100299. doi: 10.1016/j.mtla.2019.100299

Ma, F. C., Liu, P., Li, W., Liu, X. K., and Lu, W. J. (2016). The mechanical behavior dependence on the TiB whisker realignment during hot-working in titanium matrix composites. *Sci. Rep*. 6:36126. doi: 10.1038/srep 36126

Ma, F. C., Lu, S. Y., Liu, P., Li, W., Liu, X. K., and Chen, X. H. (2017a). Evolution of strength and fibers orientation of a short-fibers reinforced Ti-matrix composite after extrusion. *Mater. Des*. 126, 297–304. doi: 10.1016/j.matdes.2017.04.058

Ma, F. C., Lu, S. Y., Liu, P., Lu, W. J., and Zhang, D. (2017b). Microstructure and mechanical properties variation of TiB/Ti matrix composite by thermo-mechanical processing in beta phase field. *J. Alloy Compd*. 695, 1515–1522. doi: 10.1016/j.jallcom.2016.10.291

Ma, F. C., Wang, C. H., Liu, P., Li, W., Liu, X. K., Chen, X. H., et al. (2018). Microstructure and mechanical properties of Ti matrix composite reinforced with 5 vol.% TiC after various thermo-mechanical treatments. *J Alloy Compd*. 758, 78–84. doi: 10.1016/j.jallcom.2018.05.134

Nie, X., Liu, H. Q., Zhou, X. Z., Yi, D. Q., Huang, B. Y., Hu, Z., et al. (2016). Creep of Ti−5Al−5Mo−5V−1Fe−1Cr alloy with equiaxed and lamellar microstructures. *Mater. Sci. Eng. A* 651, 37–44. doi: 10.1016/j.msea.2015. 10.092

Ozerov, M., Klimova, M., Sokolovsky, V., Stepanov, N., Popov, A., Boldin, M., et al. (2019). Evolution of microstructure and mechanical properties of Ti/TiB metal-matrix composite during isothermal multiaxial forging. *J Alloy Compd*. 770, 840–848. doi: 10.1016/j.jallcom.2018.08.215

Pitt, F., Ramulu, M., Labossiere, P., and Young, S. (2004). Postprocessing effect on the ductility and flexural behavior of three titanium alloys under simulated superplastic forming conditions. *J. Mater. Eng. Perform*. 13, 735–743. doi: 10.1361/10599490421565

Rabadia, C. D., Liu, Y. J., Chen, L. Y., Jawed, S. F., Wang, L. Q., Sun, H., et al. (2019). Deformation and strength characteristics of Laves phases in titanium alloys. *Mater. Des*. 179:107891. doi: 10.1016/j.matdes.2019.107891

Rabadia, C. D., Liu, Y. J., Wang, L., Sun, H., and Zhang, L. C. (2018). Laves phase precipitation in Ti-Zr-Fe-Cr alloys with high strength and large plasticity. *Mater. Des*. 154, 228–238. doi: 10.1016/j.matdes.2018.05.035

Sastry, S. M. L., Pao, P. S., Sankaran, K. K., in: Kimura, H., and Izumi, O. (eds.). (1980). *Titanium Science and Technology,* Vol. 2. Kyoto: Metall. Soc. AIME, 873–886.

Su, C. Y., Zhou, C. Y., Lu, L., Li, J., Sun, P. Y., and He, X. H. (2018). Effect of temperature and dwell time on fatigue crack growth behavior of CP-Ti. *Metals* 8:1031. doi: 10.3390/met8121031

Vasanthakumara, K., Ghoshb, S., Koundinyaa, N. T. B. N., Ramaprabhub, S., and Bakshia, S. R. (2019). Synthesis and mechanical properties of TiCx and Ti(C,N) reinforced Titanium matrix *in situ* composites by reactive spark plasma sintering. *Mater. Sci. Eng. A*. 759, 30–39. doi: 10.1016/j.msea.2019.05.021

Wang, B., Huang, L. J., Geng, L., Rong, X. D., and Liu, B. X. (2015). Effects of heat treatments on microstructure and tensile properties of as-extruded TiBw/near-α Ti composites. *Mater. Des*. 85, 679–686. doi: 10.1016/j.matdes.2015.07.058

Wang, P., Qin, J. N., Lu, W. J., and Chen, Y. F. (2009). Creep behavior of *in situ* synthesized 7715D titanium matrix composite. *Mater. Trans. JIM*. 50, 1411–1417. doi: 10.2320/matertrans.MRA2008425

Wang, S., Huang, L. J., Zhang, R., Liu, B. X., Cui, X. P., Geng, L., et al. (2019). Enhancing ductility of titanium matrix composites by multimodal α-grains. *Scripta Mater*. 170, 161–165. doi: 10.1016/j.scriptamat.2019.06.009

Wang, X., Jahazi, M., and Yue, S. (2006). Substructure of high temperature compressed titanium alloy IMI 834. *Mater. Sci. Eng. A* 434, 188–193. doi: 10.1016/j.msea.2006.06.119

Xiao, L., Lu, W. J., Qin, J. N., Chen, Y. F., Zhang, D., Wang, M. M., et al. (2009). Steady state creep of *in-situ* TiB plus La$_2$O$_3$ reinforced high temperature titanium matrix composite. *Mater. Sci. Eng. A* 499,500–506. doi: 10.1016/j.msea.2008.09.002

Zhang, L. C., and Chen, L. Y. (2018). A review on biomedical titanium alloys: recent progress and prospect. *Adv. Eng. Mater*. 21:1801215. doi: 10.1002/adem.201801215

Zhang, Z. G., Qin, J. N., Zhang, Z. W., Chen, Y. F., Lu, W. J., and Zhang, D. (2010). Microstructure effect on mechanical properties of *in situ* synthesized titanium matrix composites reinforced with TiB and La2O3. *Mater. Lett*. 64, 361–363. doi: 10.1016/j.matlet.2009.11.019